Arabian Journal of Chemistry (2020) 13, 4857–4867

King Saud University

Arabian Journal of Chemistry

www.ksu.edu.sa
www.sciencedirect.com

ORIGINAL ARTICLE

# *In situ* growth of $Co_3O_4$ nano-dodecahedeons on $In_2O_3$ hexagonal prisms for toluene catalytic combustion

**Jiuhu Zhao [a,b], Weiliang Han [a], Jiyi Zhang [b], Zhicheng Tang [a,*]**

[a] *State Key Laboratory for Oxo Synthesis and Selective Oxidation, National Engineering Research Center for Fine Petrochemical Intermediates, Lanzhou Institute of Chemical Physics, Chinese Academy of Sciences, Lanzhou 730000, PR China*
[b] *School of Petroleum and Chemical, Lanzhou University of Technology, Lanzhou 730050, PR China*

Received 26 November 2019; accepted 12 January 2020
Available online 24 January 2020

**KEYWORDS**

*In-situ* growth;
ZIF-67/MIL-68;
$Co_3O_4/In_2O_3$;
Co/In molar ratio;
Toluene catalytic combustion

**Abstract** In this paper, *in situ* growth of $Co_3O_4$ nano-dodecahedra on $In_2O_3$ hexagonal prisms were synthesized via pyrolysis of ZIF-67/MIL-68. Interestingly, the amount of $Co_3O_4$ dodecahedra on $In_2O_3$ hexagonal prisms was regularly regulated and controlled. In detail, four $Co_3O_4/In_2O_3$ catalysts with various Co/In molar ratio were prepared, including $Co_4In_1$ (Co/In molar ratio was 4:1), $Co_2In_1$ (Co/In molar ratio was 2:1), $Co_1In_1$ (Co/In molar ratio was 1:1), $Co_{0.5}In_1$ (Co/In molar ratio was 0.5:1). The catalytic performance of $Co_3O_4/In_2O_3$ catalysts was systematically investigated for toluene combustion. It could be noted that the $Co_2In_1$ sample exhibited the superior catalytic performance, and the temperatures for 90% toluene conversion ($T_{90}$) was 182 °C. Furthermore, the toluene conversion of $Co_2In_1$ sample had no significant decrease at 178 °C for 15 h, indicating that it presented superior stability for toluene oxidation reaction. Through various characterizations, it was verified that the Co/In molar ratio of $Co_3O_4/In_2O_3$ catalyst could obviously alter the surface atomic ratio of $Co^{3+}/(Co^{3+} + Co^{2+})$, BET surface area, the number of surface adsorbed oxygen, the interaction between $In_2O_3$ and $Co_3O_4$ of $CoInO_x$ catalysts and so on. The lots of surface adsorbed oxygen, strong interaction between $In_2O_3$ and $Co_3O_4$ would promote the catalytic oxidation of toluene. Especially, we discovered that the catalytic activity of $Co_3O_4/In_2O_3$ was obviously improved with the increase of $Co^{3+}/(Co^{3+} + Co^{2+})$ surface atomic ratio.


## 1. Introduction

Volatile organic compounds (VOCs) are an important class of air pollutants because they are precursors to smog and ozone, causing toxicity and malodorous (Kim and Shim, 2010; Zhao et al., 2018; Zhao et al., 2019). Meanwhile, it is a class of compounds which includes carbon-based chemicals. Inhaling high

* Corresponding author.
E-mail address: tangzhicheng@licp.cas.cn (Z. Tang).
Peer review under responsibility of King Saud University.

Production and hosting by Elsevier

https://doi.org/10.1016/j.arabjc.2020.01.014
1878-5352 © 2020 The Authors. Published by Elsevier B.V. on behalf of King Saud University.

concentrations of VOCs could affect the respiratory system and could also cause blood diseases and cancer. To reduce the negative impacts on environment and human health, VOCs are worldwide supervised (Han et al., 2018; Liu et al., 2014; Kampa and Castanas, 2008; Garcia et al., 2010; Jones, 1999). It is important to develop effective materials and methods to remove VOCs. Among those conventional control processes, adsorptionbased techniques are only really suitable for controlling of highly dilute VOCs emissions (Malhautier et al., 2014; Li et al., 2011; Kołodziej and Łojewska, 2005). Absorption and membrane separation are costly (Tokumura et al., 2008; Ruddy and Carroll, 1993). Biological degradation is generally selective, concentration and temperature-sensitive, and effective only for low-weight and highly soluble hydrocarbons (Santos et al., 2007). According to the literature, catalytic combustion is regarded as one of the most effective methods because it avoids repeated contamination and operates at lower temperatures (Wu et al., 2004; Everaert and Baeyens, 2004; He et al., 2009; Papaefthimiou et al., 1997; Li et al., 2009; Tang et al., 2014; Delimaris and Ioannides, 2008).

Metal oxides are regarded as an effective catalyst, which could trigger the reaction for catalytic oxidation of VOCs at low temperature. $Co_3O_4$ has a typical spinel structure of $Co^{2+}$-$Co^{3+}O_4$, in which $Co^{3+}$ is in an octahedral coordination, $Co^{2+}$ is in tetrahedral coordination structure, and $O^{2-}$ is cubic dense. The high activity of $Co_3O_4$ may be due to the low ΔH of $O_2$ vaporization (Wang et al., 2017). Therefore, among the most common metal oxides, cobalt oxide is the most widely used for catalytic oxidation material (Han et al., 2018; Konsolakis et al., 2017). As recently reported, appropriate incorporation of metal oxides may be more active and thermally stable than the single oxides. For example, $Mn_xCo_{3-x}O_4$ (Zhao et al., 2019), $Co_{3-x}Cu_xO_4$; (Feng and Zheng, 2012) $Zn_xCo_{1-x}Co_2O4$ (Marcos et al., 2013) and $NiO_x$, $CrO_x$ and $Bi_2O_3$ modified $Co_3O_4$ (Yan et al., 2003; Zhao et al., 2012; Lou et al., 2011) exhibited higher activity than pure $Co_3O_4$. In addition, Lou et al. prepared $In_2O_3/Co_3O_4$ catalysts for ultralowtemperature CO oxidation by simultaneously tuning the CO adsorption strength and oxygen activation over a $Co_3O_4$ surface, which could completely convert CO to $CO_2$ at temperatures as low as −105 compared to 40 over pure $Co_3O_4$. The doping of $In_2O_3$ significantly promoted the catalytic performance of $Co_3O_4$ for CO oxidation (Lou et al., 2014). According to a series of characterization, it could be inferred that the doping of $In_2O_3$ induced the structural defects, modified the surface electronic structure, and promoted the redox ability of $Co_3O_4$, which tuned the adsorption strength of CO and oxygen activation simultaneously (Lou et al., 2014).

Recently, metal organic frameworks (MOFs) have gained extensive consideration to synthesize porous materials (Cai et al., 2015). MOFs has been studied as potential application in various fields owing to the unique architectures and versatile functionalities (Wang et al., 2015; Koo et al., 2017). Zeolitic imidzolate frameworks (ZIFs) are a highly ordered porous soilds (Luo et al., 2018; Ding et al., 2017; Tsai and Langner, 2016). ZIF-67 has been considered a typical ZIF species (Shi et al., 2011). Furthermore, MIL-n materials are a class of MOFs derived from trivalent metal cations such as $Al^{3+}$, $Cr^{3+}$, $V^{3+}$, $In^{3+}$ or $Ga^{3+}$ and carboxylic acid groups (Jin et al., 2015). Compared with activated carbon and zeolite, MOFs materials have many advantages, including huge specific surface area, order pore structure, diverse pore surface functional group and surface potential energy. Thus, the application of MOFs materials to VOCs field has board prospects (Yang et al., 2012). As we know; almost few research on the application of $Co_3O_4/In_2O_3$ with different Co/In molar ratio synthesized by pyrolysis of ZIF-67/MIL-68 as the catalyst supports for VOCs.

In the work, four samples of $Co_3O_4/In_2O_3$ with different Co/In molar ratio were synthesized. Moreover, the catalytic performance was investigated by toluene combustion. The effect of morphology was extensively characterized on the catalytic performance.

## 2. Results and discussion

### 2.1. Morphology of the catalysts

Fig. 1a and b was SEM images of ZIF-67/MIL-68 (In) nanocrystals. Obviously, MIL-68 nanocrystals had a regular hexagonal prisms shape with high uniformity, the average size was about 1.7 μm. ZIF-67 presented the appearance of dodecahedron, which grew *in situ* on the surface of MIL-68 nanocrystals. Fig. 1b-e were SEM images of $Co_4In_1$, $Co_2In_1$,

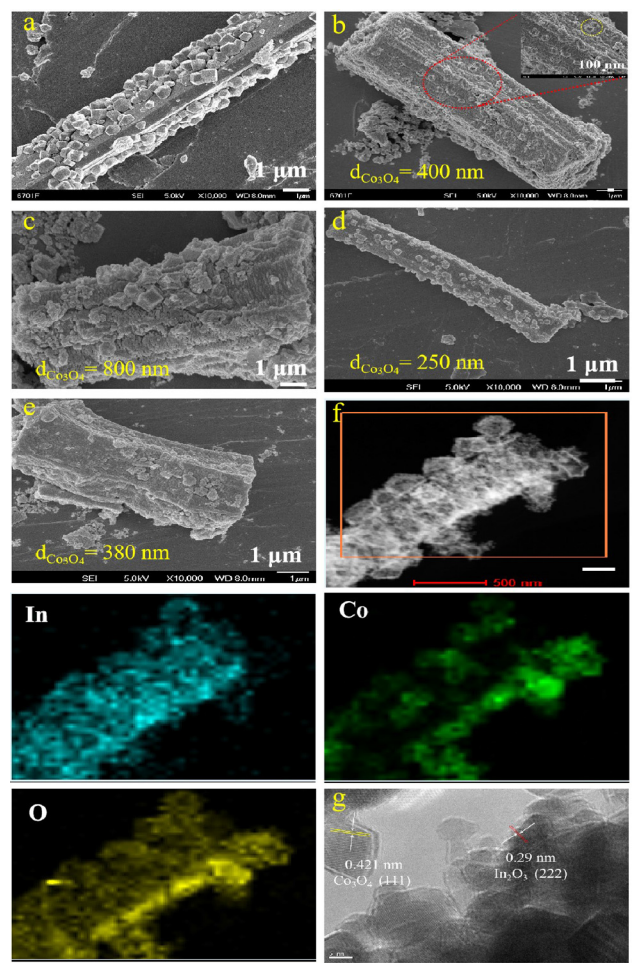


**Fig. 1** SEM image of the as-prepared ZIF-67/MIL-68(In) (a), $Co_4In_1$ (b), $Co_2In_1$ (c), $Co_1In_1$ (d) and $Co_{0.5}In_1$ (e); TEM image of EDS mapping images of $Co_2In_1$ (f) and the HRTEM image of $Co_2In_1$ (g).

$Co_1In_1$ and $Co_{0.5}In_1$, respectively. After the calcination treatment at 400 °C for 2 h with a heating rate of 1 °C $min^{-1}$ in air, it was discovered that the mass of $Co_3O_4/In_2O_3$ well inherited the morphology and uniformity of ZIF-67/MIL-68, while a small number of $Co_3O_4$ dodecahedra and $In_2O_3$ hexagonal prisms collapsed in process of pyrolysis of ZIF-67/MIL-68. Nevertheless, the samples presented concave and plicated appearance. Moreover, the amount of $Co_3O_4$ dodecahedra on $In_2O_3$ hexagonal prisms was different, notably. The quantity of $Co_3O_4$ followed the order: $Co_4In_1$ > $Co_2In_1$ > $Co_1In_1$ > $Co_{0.5}In_1$. Meanwhile, the particle size of $Co_3O_4$ nanoparticles of four catalysts were different. Thus, it could be rational reduced that the quantity of $Co_3O_4$ affected the the particle size of $Co_3O_4$ nanoparticles of four catalysts.

Fig. 1f showed the elemental mapping image of $Co_2In_1$ sample manifested that O element was uniformly distributed in the nanocrystals. Meanwhile, In element was distributed in the hexagonal prisms and dodecahedra while Co element was uniformly distributed in the dodecahedra. It could be inferred the In element on the surface of the hexagonal prisms was migrated or dissolved when *in situ* growth of $Co_3O_4$ nano-dodecahedra on $In_2O_3$ hexagonal prisms. Fig. 1g showed the HRTEM image of the as-prepared $Co_2In_1$ sample. The $Co_2In_1$ showed the $Co_3O_4$ (1 1 1) and $In_2O_3$ (2 2 2) crystalline plane with lattice distances of 0.421 nm and 0.29 nm, respectively.

### 2.2. Texture properties of the catalysts

XRD analysis was conducted to study the structural properties of the $Co_4In_1$, $Co_2In_1$, $Co_1In_1$ and $Co_{0.5}In_1$ catalysts. As shown in Fig. 2a, the diffraction peaks at 19.0°, 36.9°, 44.8°, 59.3° and 65.2° were corresponding to the (1 1 1), (3 1 1), (4 0 0), (5 1 1) and (4 4 0) of $Co_3O_4$ (PDF#42-1467). The detectable reflections were consistent with standard data of cubic phase $Co_3O_4$, indicating that ZIF-67 has been successfully transformed into $Co_3O_4$. In addition, The diffraction peaks at 21.5°, 30.6°, 35.4°, 41.8°, 46.7°, 51.0° and 60.6° were corresponding to the (2 1 1), (2 2 2), (4 0 0), (3 3 2), (4 3 1), (4 4 0) and (6 2 2) of $In_2O_3$ (PDF#06-0416), suggesting that the MIL-68 has been successfully transformed into $In_2O_3$ (Chen et al., 2018). Obviously, with the increase of the molar ratio of In to Co, it could be seen that the diffraction peaks of $Co_3O_4$ tended to weak while the diffraction peaks of $In_2O_3$ strengthened. Contacted to the SEM, $Co_3O_4$ well inherited the dodecahedron morphology of ZIF-67 and $In_2O_3$ exhibited the hexagonal prisms morphology of MIL-68, sug-

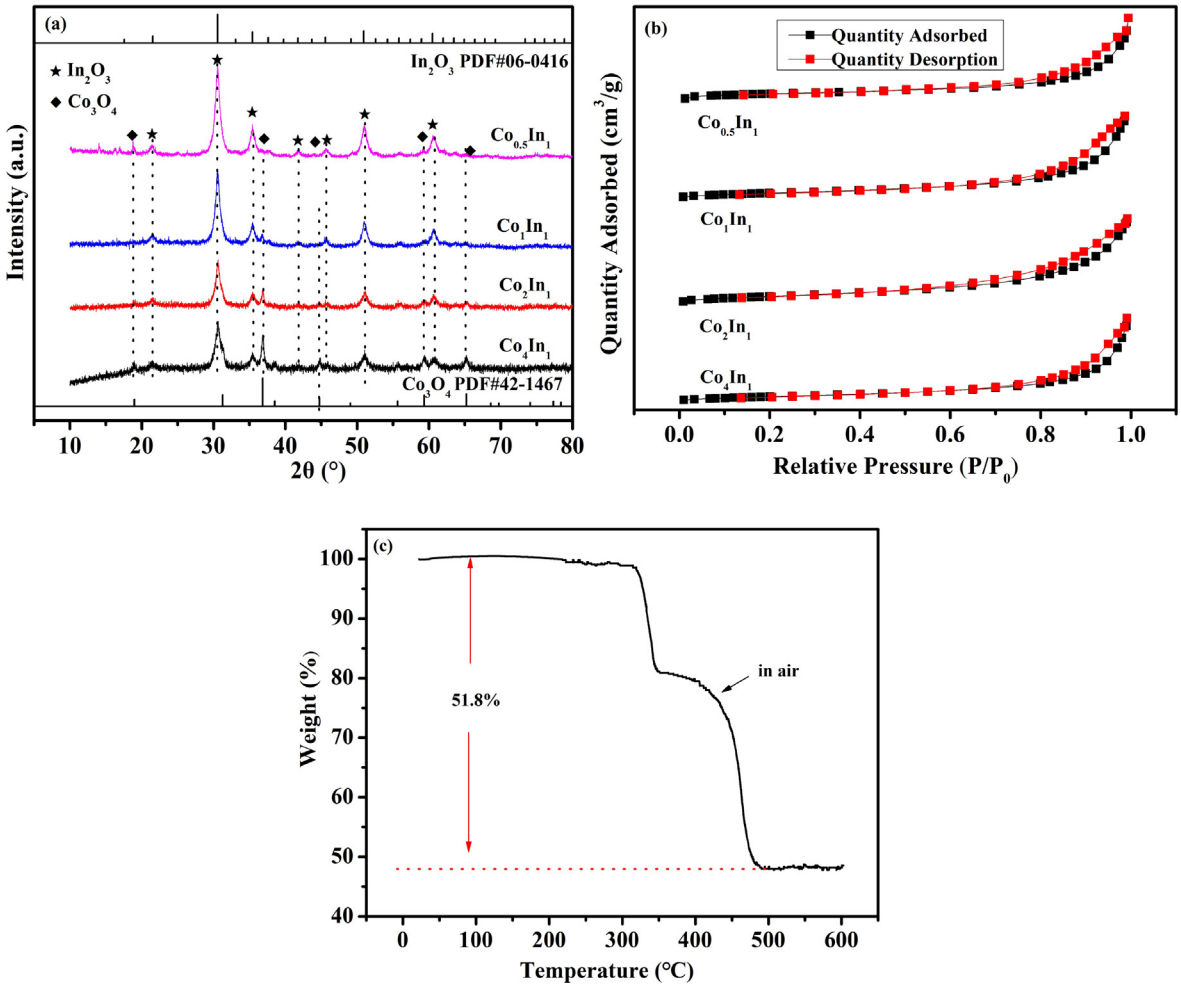


**Fig. 2** XRD pattern of $Co_4In_1$, $Co_2In_1$, $Co_1In_1$ and $Co_{0.5}In_1$ (a); $N_2$ adsorption–desorption isotherms of $Co_4In_1$, $Co_2In_1$, $Co_1In_1$ and $Co_{0.5}In_1$ (b) and TG curves of the ZIF-67/MIL-68 (2:1) in air (c).

gesting that the structure of $In_2O_3$ and $Co_3O_4$ was unbroken. Moreover, the incorporation of In into the $Co_3O_4$ structure would inevitably result in lattice distortion due to the difference in ionic radius and electronic state. By applying the Scherrer equation, the crystallite size could be also calculated from the $In_2O_3$ (2 2 2) diffraction peak (Luo et al., 2018; Chen et al., 2018; Wei et al., 2010). The results were shown in Table 1. The crystallite size of $Co_4In_1$; $Co_2In_1$, $Co_1In_1$ and $Co_{0.5}In_1$ catalysts was 13.64 nm, 12.14 nm, 13.71 nm and 12.87 nm, respectively.

The $N_2$ adsorption–desorption isotherms of the $Co_4In_1$, $Co_2In_1$, $Co_1In_1$ and $Co_{0.5}In_1$ catalysts was shown in Fig. 2b. By the IUPAC, the $N_2$ adsorption–desorption isotherms of four catalysts could be divided to type Ⅳ with H3 hysteresis loop, which due to the capillary condensation, the adsorption branch of isotherms at higher relative pressure was inconsistent with the desorption branch. Table 1 showed the average pore diameters, pore volumes and BET surface areas of $Co_4In_1$, $Co_2In_1$, $Co_1In_1$ and $Co_{0.5}In_1$ catalysts. The BET surface areas of the $Co_4In_1$, $Co_2In_1$, $Co_1In_1$ and $Co_{0.5}In_1$ were 63.07, 75.58, 67.07, and 68.53 $m^2\ g^{-1}$, respectively. Easy to see, the BET surface areas of four catalysts were almost similar. Thus, the main factor was not the BET surface areas, which affect the catalytic performance. In addition, $Co_2In_1$ sample showed the larger average pore diameter (16.1 nm) than that of $Co_4In_1$ sample (11.3 nm) $Co_1In_1$ (15 nm) and $Co_{0.5}In_1$ sample (14.9 nm). In catalytic oxidation of toluene process, these porous structures could be beneficial for toluene molecules to quickly penetrate into the pores and contact to active sites.

The TG curves of ZIF-67/MIL-68 (4:1) were showed in Fig. 2c. In the temperature range of 310–500 °C, not hard to see, ZIF-67/MIL-68 (2:1) had a sharply weight loss by two step. The total weight loss from 310 °C to 500 °C was 51.8% in the decomposition process. In the temperature range of 310–350 °C, it was concluded that the weight change in the transformation from ZIF-67 to $Co_3O_4$, which was regarded as resulting from desorption of surface adsorbed OH, water and decomposition of 2-MIM. In the temperature range of 350–500 °C, the TG curve was well represented by the weight change in the transformation from MIL-68 to $In_2O_3$ and the stoichiometry of $Co_3O_4$ decompositions, which could be attributed to the stoichiometry of decomposition of 1,4-dicarboxybenzene and lattice oxygen loss from $Co_3O_4$. It could be concluded that large amounts of $CO_2$, $H_2O$ and $NO_x$ would be released in the decomposing process of the ZIF-67/MIL-68.

### 2.3. Chemical states and redox behavior

The Co 2p, In 3d and O 1s XPS spectra of four catalysts were shown in Fig. 3. In the Co 2p spectrum of four samples, two main peaks at 780 eV and 795 eV were observed, corresponding to Co $2p_{3/2}$ and Co $2p_{1/2}$, respectively. The fitting peaks at binding energies of 781.2 eV and 796.6 eV were related to $Co^{2+}$, while another fitting peaks of 780.0 eV and 795.1 eV were related to $Co^{3+}$ (Bao et al., 2018). Meanwhile, it could be seen that the satellite peaks were located on 786.3 eV and 804.3 eV. Table 2 exhibited the $Co^{3+}/(Co^{3+}+Co^{2+})$ ratios. The relative ratio of $Co^{3+}/(Co^{3+}+Co^{2+})$ that was calculated using the curve-fitted data, which were 0.43, 0.49, 0.41 and 0.44 respectively. It was found that the ratio of $Co^{3+}/(Co^{3+}+Co^{2+})$ conformed the order of $Co_2In_1 > Co_{0.5}In_1 > Co_4In_1 > Co_1In_1$.

Fig. 3b displayed the XPS spectra in the In 3d region of the four samples. Generally, the In 3d peaks were composed of two main spin-orbital lines, In $3d_{5/2}$ and In $3d_{3/2}$ peaking at 452.1 and 444.6 eV (Lou et al., 2014). The In $3d_{3/2}$/(In $3d_{5/2}$ + In $3d_{3/2}$) ratios were also exhibited in Table 3. The relative ratio of In $3d_{3/2}$/(In $3d_{5/2}$ + In $3d_{3/2}$) that was calculated using the curve-fitted data decreased, which were 0.45, 0.45, 0.45 and 0.45 respectively. It was discovered that the ratio of In $3d_{3/2}$/(In $3d_{5/2}$ + In $3d_{3/2}$) had no difference.

Fig. 3c showed the XPS spectra of O 1s. The O 1s XPS of four catalysts could be fitted by three peaks. The peaks at binding energies of around 529.6, 530.6, 532.1 eV was assigned to the surface lattice oxygen in the lattice oxygen ($O_\alpha$), chemical adsorption oxygen ($O_\beta$), adsorbed water/OH ($O_\gamma$), respectively. It was generally accepted that the charge on the oxide ions was significantly influenced by their surrounding chemical environment, and the nature of dopant ions would decide the shifts of O 1s binding energy to either side (Shang et al., 2017). It was rationally deduced that there existed the strong interaction of two oxides in $Co_3O_4/In_2O_3$. Furthermore, the chemical adsorption oxygen species played a significance part in catalytic oxidation. The more $O_\beta$ species exhibited, the better catalytic activity was discovered. Table 2 exhibited the $O_\beta/(O_\alpha + O_\beta + O_\gamma)$ ratio. For $Co_4In_1$, $Co_2In_1$, $Co_1In_1$ and $Co_{0.5}In_1$, the surface atomic ratio of $O_\beta/(O_\alpha + O_\beta + O_\gamma)$ were 0.31, 0.37, 0.24 and 0.33, respectively.

The Raman spectra of four samples were shown in Fig. 4a. Five distinct peaks were located at 192, 477, 521, 613 and 678 $cm^{-1}$, which were consistent with the position and width of $Co_3O_4$ (Bahlawane et al., 2009). The band at 192 $cm^{-1}$ was attributed to the characteristics of tetrahedral sites ($CoO_4$), corresponding to $F^1_{2g}$ symmetry. The band at 678 $cm^{-1}$, corresponding to the $A_{1g}$ mode, was attributed to the octahedral sites ($CoO_6$) in the $O^7_h$ symmetry. The weak band at 613 $cm^{-1}$ was associated with the $F^2_{2g}$ mode, the Raman modes at 477 $cm^{-1}$ and 521 $cm^{-1}$ was respectively symmetries of $F^2_{2g}$ and $E_g$ mode, which resulted from the vibration of tetrahedral and octahedral sites. Nevertheless, no position and width was consistent with the spinel of $In_2O_3$. Compared with $Co_4In_1$, $Co_1In_1$ and $Co_{0.5}In_1$ catalysts,

**Table 1** Crystallite size and pore structure parameters of $Co_4In_1$, $Co_2In_1$, $Co_1In_1$ and $Co_{0.5}In_1$.

| Samples | BET surface area[a] ($m^2\ g^{-1}$) | Pore volume[a] ($cm^3 g^{-1}$) | Average pore diameter[a] (nm) | Crystallite size[b] (nm) |
|---|---|---|---|---|
| $Co_4In_1$ | 63.07 | 0.21 | 11.3 | 13.64 |
| $Co_2In_1$ | 75.58 | 0.26 | 16.1 | 12.14 |
| $Co_1In_1$ | 67.07 | 0.26 | 15 | 13.71 |
| $Co_{0.5}In_1$ | 68.53 | 0.38 | 14.9 | 12.87 |

[a] From the $N_2$ adsorption–desorption isotherms of the $Co_4In_1$, $Co_2In_1$, $Co_1In_1$ and $Co_{0.5}In_1$ catalysts.
[b] The crystallite size was calculated from the $In_2O_3$ (2 2 2) diffraction peak by applying the Scherrer equation.

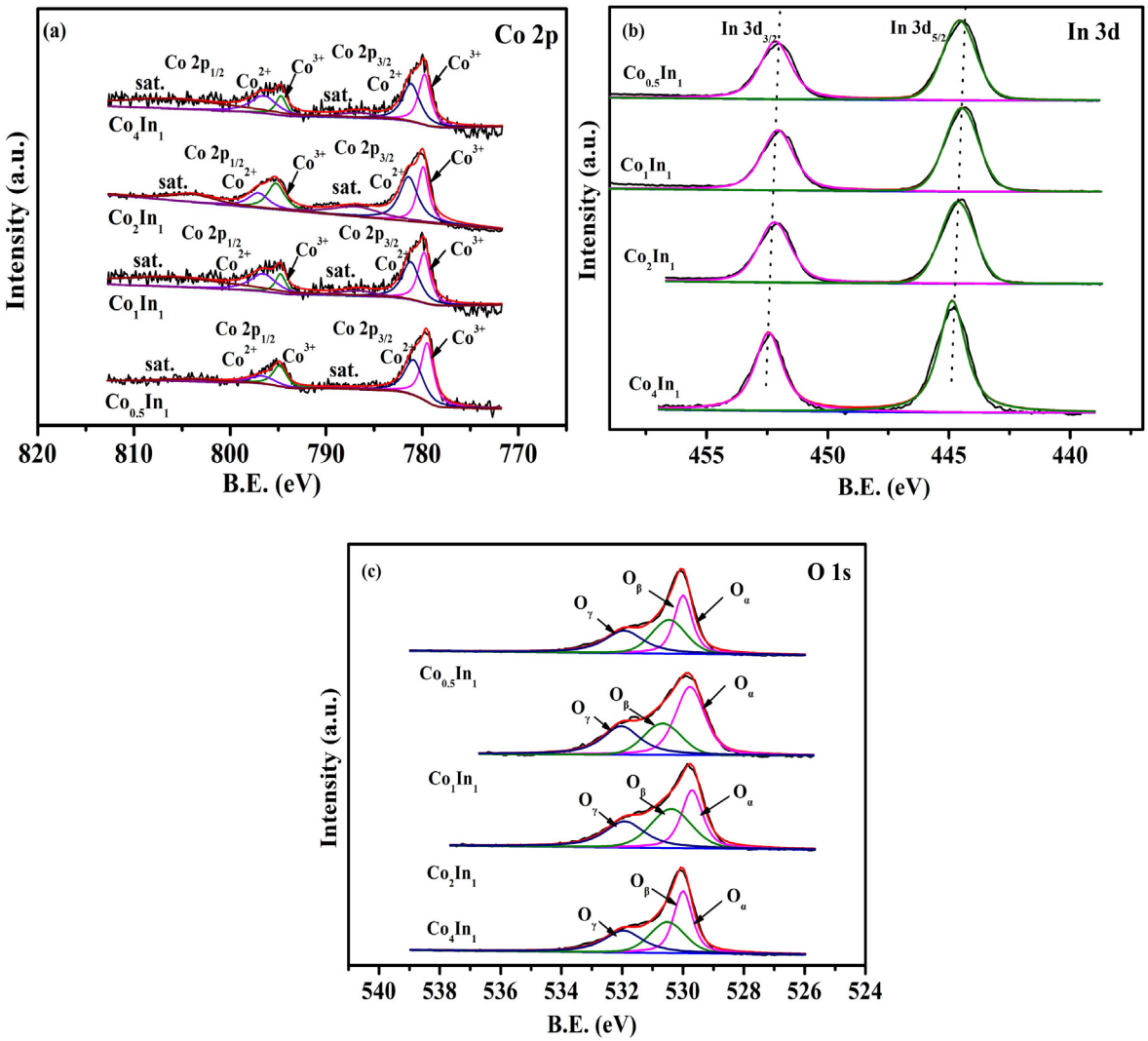


**Fig. 3** The Co 2p (a), In 3d (b), O 1s (c) XPS spectra of $Co_4In_1$, $Co_2In_1$, $Co_1In_1$ and $Co_{0.5}In_1$ catalysts.

**Table 2** Surface element compositions of $Co_3O_4/In_2O_3$ materials by XPS analysis.

| Sample | $Co^{3+}/(Co^{3+}+Co^{2+})$ | $O_\beta/(O_\alpha+O_\beta+O_\gamma)$ | In $3d_{3/2}$/(In $3d_{5/2}$ + In $3d_{3/2}$) |
|---|---|---|---|
| $Co_4In_1$ | 0.43 | 0.31 | 0.45 |
| $Co_2In_1$ | 0.49 | 0.37 | 0.45 |
| $Co_1In_1$ | 0.41 | 0.24 | 0.45 |
| $Co_{0.5}In_1$ | 0.44 | 0.33 | 0.45 |
| Used $Co_2In_1$ | 0.47 | 0.35 | 0.45 |

**Table 3** Toluene catalytic oxidation performance of the catalysts at WHSV = 30,000 mL $g^{-1}h^{-1}$.

| Samples | Reaction temperature (°C) | | Ea (kJ $mol^{-1}$) |
|---|---|---|---|
| | $T_{50}$ | $T_{90}$ | |
| $Co_4In_1$ | 176 | 208 | 132 |
| $Co_2In_1$ | 159 | 182 | 88 |
| $Co_1In_1$ | 167 | 224 | 136 |
| $Co_{0.5}In_1$ | 164 | 200 | 130 |
| $Co_3O_4$ | 244 | 260 | / |

the strongest symmetry, $A_{1g}$, in the $Co_2In_1$ sample slightly shifted to lower wave-numbers as well as described red shift. Generally speaking, red shift narrow peaks indicated that the sample had a highly defective structure. It was vitally significant to activate absorbed oxygen molecules (Ren et al., 2018).

Characteristic functional groups of the synthesized ZIF-67/MIL-68 were verified by FT-IR spectra. The adsorption peaks in the range of 500–4000 $cm^{-1}$ for ZIF-67/MIL-68 (4:1, 2:1, 1:1, 0.5:1) were shown in Fig. 4b. It was well known that ZIF-67 were derived from the stretching ligand of 2-MIM, and the peaks at 1568 $cm^{-1}$ and 2936 $cm^{-1}$ were assigned to

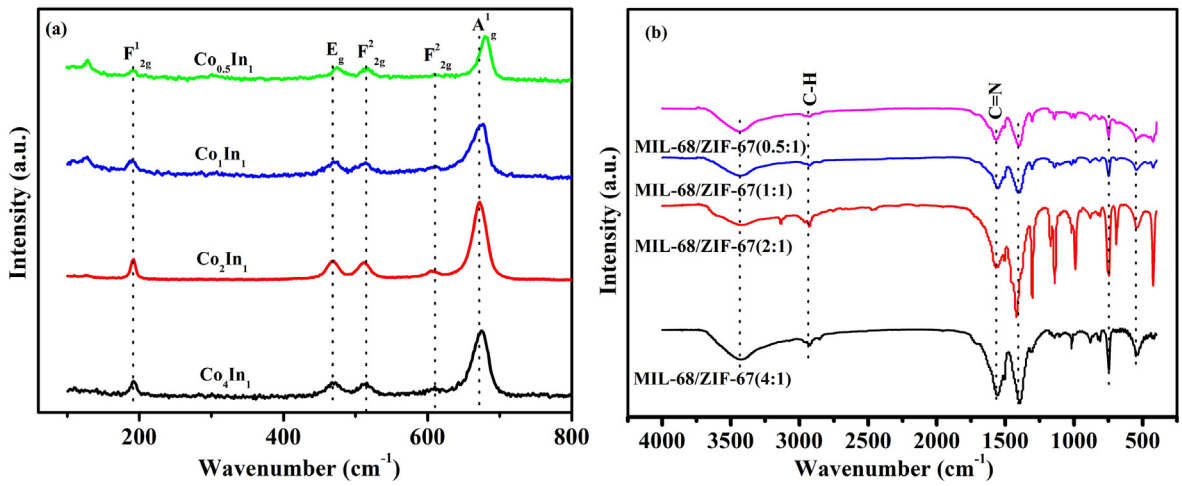


**Fig. 4** Raman spectra of $Co_4In_1$, $Co_2In_1$, $Co_1In_1$ and $Co_{0.5}In_1$ (Fig. 7a) and FT-IR spectra of $Co_4In_1$, $Co_2In_1$, $Co_1In_1$ and $Co_{0.5}In_1$ (Fig. 7b).

the stretching modes of the C=N and C-H bonds in 2-MIM. It was obvious that the strength of bonds tended to decrease from ZIF-67/MIL-68 (4:1) to ZIF-67/MIL-68 (0.5:1). It was verified that bonds strength was proportional to the amount of 2-MIM added.

The oxidation–reduction properties of the four samples were studied by $H_2$-TPR. Fig. 5 illustrated the results of the four samples. It was observed that there were four reduction peaks. The first weak peak centered at 100–130 °C could be related to active surface oxygen species (Xie and Shen, 2009; Davies et al., 2006). The second reduction peak should be the reduction of $Co_3O_4$ to CoO ($Co_3O_4 + H_2 \rightarrow 3CoO + H_2O$), and the third reduction peak should be the reduction of CoO to metallic cobalt ($3CoO + 3H_2 \rightarrow 3Co + 3H_2O$) (Ji et al., 2009). The fourth weak peak could be assigned to the reduction process of $In_2O_3$ to metallic indium for the case of $In_2O_3$ reducation. As shown in Fig. 5, it was observed that the different peak position of these four samples was caused by different moral ratio of Co to In. Compared to other catalysts, the active surface oxygen (peak I) $Co^{3+}$ reduction (peak II) $Co^{2+}$ reduction (peak III) and of $Co_2In_1$ catalyst shifted to lower temperatures at *l*01 °C and 368 °C, respectively. The shift of these reduction peaks was generally recognized as a sign of the improved reducibility of $Co^{3+}$ to $Co^{2+}$. Meanwhile, $Co_2In_1$ catalyst owned the more active surface oxygen. Nevertheless, the $In^{3+}$ reduction peak (peak IV) shifted to a higher temperature around 700 °C. The shifted of peak locations indicated the presence of strong interactions between cobalt oxide and indium oxide (Ma et al., 2018). In general, a catalyst with small crystallite size showed superior reduction capacity. Thus, the $Co_2In_1$ sample displayed excellent reducibility due to smallest crystallite size. Because of more adsorbed oxygen species, it could clearly be noticed that the $Co_2In_1$ catalyst might exhibit superior catalyst activity.

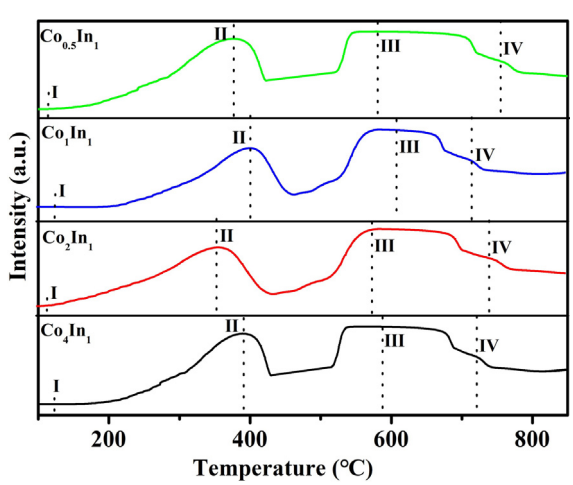


**Fig. 5** $H_2$-TPR profiles of different catalysts.

### 2.4. Catalytic performance of toluene oxidation

#### 2.4.1. Catalytic activity

The catalytic activity curves of $Co_4In_1$, $Co_2In_1$, $Co_1In_1$ and $Co_{0.5}In_1$ and pure $Co_3O_4$ catalysts was shown in Fig. 6a, and the temperatures for 50%, 90% and 100% toluene conversion ($T_{50}$, $T_{90}$ and $T_{100}$) of four catalysts were listed in Table 3. It could be observed that the conversions of toluene increased with a rise of the reaction temperature. $T_{50}$ of $Co_4In_1$, $Co_2In_1$, $Co_1In_1$, $Co_{0.5}In_1$ and $Co_3O_4$ catalysts were 176, 159, 167, 164 and 244 °C, while $T_{90}$ of $Co_4In_1$, $Co_2In_1$, $Co_1In_1$, $Co_{0.5}In_1$ and $Co_3O_4$ catalysts were 208, 182, 224, 200 and 260 °C, respectively, indicating that the performance of catalysts was the order of $Co_2In_1 > Co_{0.5}In_1 > Co_4In_1 > Co_1In_1 > Co_3O_4$ catalysts. It could be inferred that $Co_3O_4/In_2O_3$ catalysts presented the superior catalytic performance due to the presence of $In_2O_3$. In addition, the differences distinctly depended on the various moral ratio of Co to In, indicating that the choice of suitable moral ratio played an important role in determining the activity of toluene oxidation. Table 4 summarized the comparation of catalytic activity on these samples and the former literatures for toluene oxidation. For example, Co-Mn (1:1) ($T_{90}$ = 240 °C) (Luo et al., 2018), $Co_3O_4$-0.01 ($T_{90}$ = 226 °C) (Li et al., 2018), 7.4 Au/$Co_3O_4$ microspheres ($T_{90}$ = 250 °C) (Yang et al., 2014), $Co_3O_4$-KIT-6 ($T_{90}$ = 233 °C) (Du et al.,

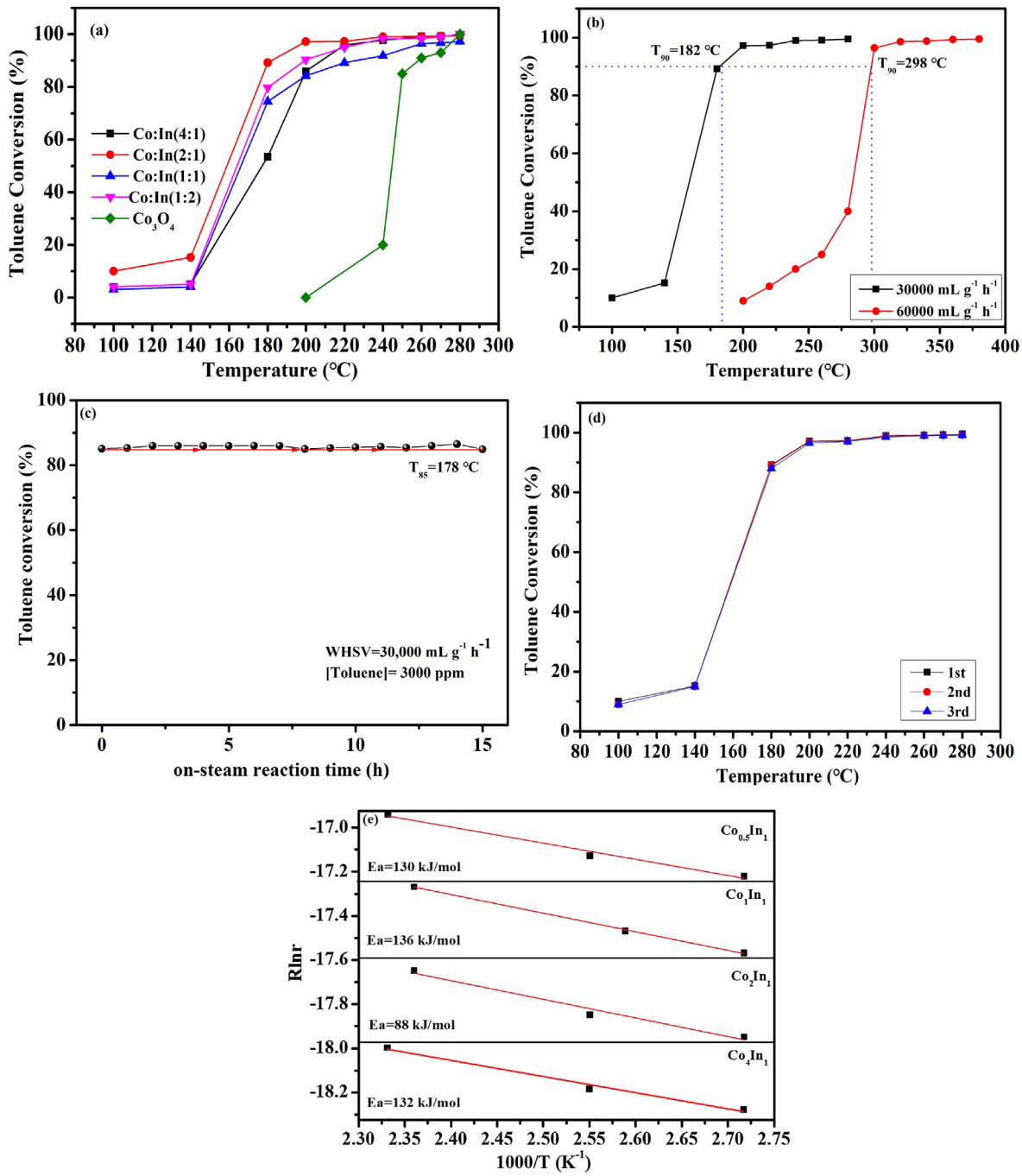


**Fig. 6** (a) Catalytic performance for toluene oxidation (b) Effect of weight hourly space velocity on toluene oxidation over the $Co_2In_1$ sample. (c) Stability tests on $Co_2In_1$. (d) The toluene conversion during three consecutives runs using $Co_2In_1$ sample. (e) Arrhenius plots of toluene catalytic oxidation reaction over $Co_4In_1$, $Co_2In_1$, $Co_1In_1$ and $Co_{0.5}In_1$ catalysts.

2012), $Co_3O_4$-HT ($T_{90}$ = 260 °C) (Bai and Li, 2014). Compared to the previous literature, $Co_2In_1$ catalyst presented excellent catalytic performance.

Fig. 6b showed the influence of weight hourly space velocity (WHSV) for the toluene reaction over $Co_2In_1$ catalyst. Because of the increase of retention time of toluene in the catalyst bed, the complete conversion temperature of toluene increased with the decrease of WHSV from 60,000 to 30000 mL $g^{-1}h^{-1}$. When the WHSV was 30,000 and 60000 mL $g^{-1}h^{-1}$, the total conversion temperature ($T_{100}$) was 182 and 298 °C, respectively. The $Co_2In_1$ catalyst exhibited superior catalytic performance at the lower WHSV, suggesting that the WHSV greatly influenced on the performance of $Co_2In_1$ catalyst.

The phenomenon about different on catalytic activity of four $Co_3O_4/In_2O_3$ catalysts might be explained by catalysts synthesis and characterization. From $N_2$ adsorption–desorption analysis, the $Co_2In_1$ catalyst exhibited larger specific surface area, thus it showed better catalytic activity.

**Table 4** The oxidation of toluene over Co-based catalysts.

| samples | Surface area($m^2$ $g^{-1}$) | VOC type | VOC conc. (ppm) | WHSV (mL $g^{-1}h^{-1}$) | $T_{50\%}$ (°C) | $T_{90\%}$ (°C) | Ref. no. |
|---|---|---|---|---|---|---|---|
| Mn-Co (1:1) | 27.9 | Toluene | 500 | 96,000 | 226 | 240 | 36 |
| $Co_3O_4$-0.01 | 56 | Toluene | 1000 | 15,000 | 217 | 226 | 53 |
| 7.4 Au/$Co_3O_4$ microspheres | 22.4 | Toluene | 1000 | 20,000 | 242 | 250 | 54 |
| $Co_3O_4$-KIT6 | 102 | Toluene | 1000 | 20,000 | 228 | 233 | 55 |
| $Co_3O_4$-HT | 41.9 | Toluene | 1000 | 20,000 | 241 | 260 | 56 |
| $Co_2In_1$ | 75.58 | Toluene | 3000 | 30,000 | 159 | 182 | Present work |

Furthermore, the higher surface $Co^{3+}$ species and surface chemical adsorbed oxygen of $Co_2In_1$ catalyst were advantageous to the reaction of toluene oxidation. Thus, the combination of these effects usually leads to the superior catalytic activity of $Co_2In_1$ catalyst in reaction of toluene oxidation. According to XRD, XPS and Raman, cobalt oxide spinel-type crystallites included both $Co^{2+}$ in tetrahedral and $Co^{3+}$ in octahedral positions. Active centers of oxidation were formed in octahedral positions, it could be benificial to form oxygen vacancies in electron transferred progress, which boost absorption of toluene molecules in the catalytic oxidation cycle (Ma et al., 2018). Thus $Co^{3+}$ which located at a relatively opened coordination position could be a centre of oxygen adsorption and formation of active oxygen species which were a precondition for catalytic oxidation. The $Co_2In_1$ catalyst had the higher surface $Co^{3+}$ species, thus it exhibited superior catalytic activity. The surface chemical adsorbed oxygen played an extremely important role on toluene oxidation. It could be observed that the $Co_2In_1$ catalyst owned the more surface $O_\beta$ species and $O_\beta/(O_\alpha + O_\beta + O_\gamma)$ atomic ratios was directly proportional to catalytic activity. Therefore, this was a reason that $Co_2In_1$ catalyst possessed excellent catalytic activity in reaction of toluene oxidation. In addition, a weak reduction peak was observed from $H_2$-TPR, it attested the molecular oxygen species adsorbed on the oxygen vacancies, which consistent with XPS. The oxygen vacancy could active the $O_2$ and promote catalytic oxidation, simultaneously. Furthermore, the strong interactions between cobalt oxide and indium oxide influenced the catalytic activity in toluene catalytic oxidation. Besides, the $Co_2In_1$ catalyst had smallest crystallite size, leading to strong reducibility. Low temperature reducibility could enhance the catalytic performance of this catalyst. All of these factors determined that the $Co_2In_1$ catalyst presented excellent catalytic activity for toluene catalytic oxidation.

### 2.4.2. Stability

The suitability of a catalyst for VOCs catalytic combustion was influenced by a limited or ideally negligible ability to yield by-products coming from an incomplete conversion of the feed. At lower reaction temperatures, although no CO was noticed, significant amounts of benzoic acid benzaldehyde and benzyl alcohol were detected. However, catalysts showed a comparable excellent selectivity to $CO_2$ (100%) at the temperature for 100% toluene conversion. Furthermore, the best $Co_2In_1$ catalyst was selected to evaluate its thermal stability, and the results were exhibited in Fig. 6. The thermal lifetime experiments of the $Co_2In_1$ were investigated and shown in Fig. 6c. It was obvious that the curve fluctuates in 85% ranges. Hence, the $Co_2In_1$ catalyst at 178 °C was stable over the period of 15 h, perfectly. In summary, $Co_2In_1$ catalyst had excellent thermal stability. As shown in Fig. 6d, it was discovered that there was almost no differences between the three curves, suggesting that the $Co_2In_1$ catalyst presented similar catalytic activity. Therefore, it was concluded that the $Co_2In_1$ catalyst had favorable performance in the catalytic cycling for toluene combustion.

It was well known that the rate of chemical reaction was associated with the activation energy. By reducing the activation energy, some slow reactions would be promoted. The Arrhenius plots for toluene oxidation over three samples reaction were studied. The detail calculation method was shown in supporting information. As shown in Fig. 6e, all profiles exhibited excellent linear relations between ln r and 1000/T and the $E_a$ of the $Co_2In_1$ catalysts were listed in Table 3. The $Co_2In_1$ catalyst had the lower $E_a$ (Ea = 88 kJ $mol^{-1}$) than $Co_4In_1$ catalyst (Ea = 132 kJ $mol^{-1}$), $Co_1In_1$ catalyst (Ea = 136 kJ $mol^{-1}$) and $Co_{0.5}In_1$ catalyst (Ea = 130 kJ $mol^{-1}$). It was obvious that the catalytic activities followed an inverse trend with respect to the $E_a$ values. Thus, the results confirmed that the $Co_2In_1$ exhibited the superior catalytic activity.

### 2.4.3. The texture and chemical properties after toluene oxidation reaction

XPS results of $Co_2In_1$ catalyst after three consecutive runs (used $Co_2In_1$) were presented in Fig. 7. The Co 2p XPS results of the catalyst could also be curve-fitted into 2 components, which were characteristic of $Co^{3+}$ (low energy) and $Co^{2+}$ (high energy). The above work confirmed that the ratio of $Co^{3+}/(Co^{3+}+Co^{2+})$ could influence the catalytic activity of catalyst. It was discovered that there was no difference between the fitting peaks of fresh and used $Co_2In_1$ catalyst at binding energies. Furthermore, according to Table 2, the ratios of $Co^{3+}/(Co^{3+}+Co^{2+})$ were 0.49 and 0.47, indicating that $Co^{3+}$ cations were the dominant species in $Co_3O_4$ spinel oxide. As shown in Fig. 7b, the O 1s XPS of used $Co_2In_1$ catalyst could be fitted by three peaks as well. The peaks at binding energies of around 529.6, 530.6, 532.1 eV was assigned to the surface lattice oxygen in the lattice oxygen ($O_\alpha$), chemical adsorption oxygen ($O_\beta$), adsorbed water/OH ($O_\gamma$), respectively. According to Table 3, the ratios of $O_\beta/(O_\alpha+O_\beta + O_\gamma)$ were 0.37 and 0.35, indicating that the surface adsorption oxy-

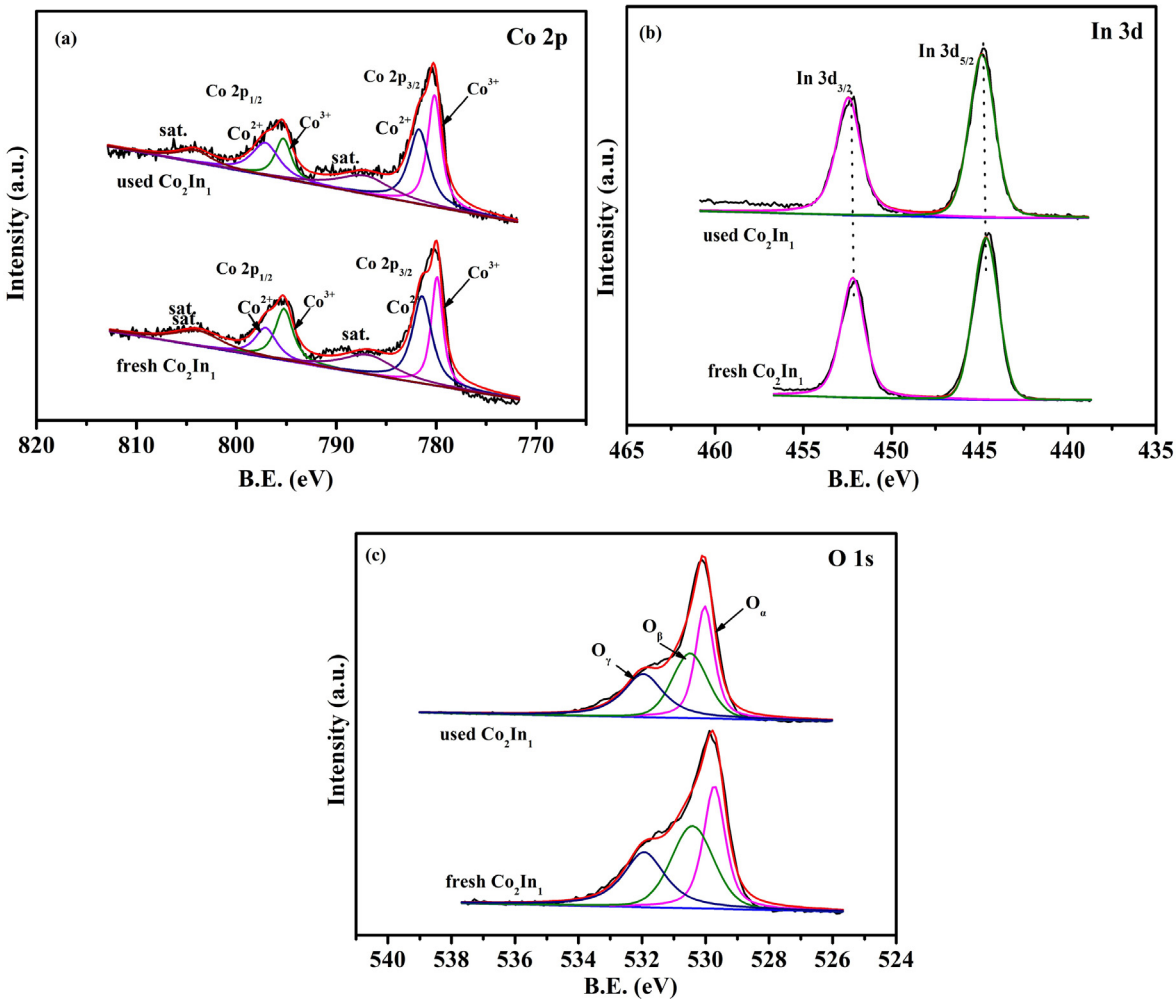


**Fig. 7** Co 2p, In 3d and O 1s XPS spectra of $Co_2In_1$ catalyst before and after reaction.

gen was not much less. Thus, the $Co_2In_1$ catalyst had favorable performance in the catalytic cycling of toluene oxidation.

### *2.4.4. Proposed reaction mechanism*

According to the above results and literature (Han et al., 2018; Kamal et al., 2016), chemically adsorbed oxygen played an important role and $Co^{3+}$ transformed to $Co^{2+}$ in the catalytic reaction of toluene combustion. Thus, Langmuir-Hinshelwood (L-H) mechanism was considered for the toluene oxidation process, preferentially. The L-H mechanism assumed that the reaction occurred between the adsorbed molecular, including the adsorbed VOCs and the adsorbed oxygen species. Therefore, both the VOCs and oxygen molecule must be adsorbed on the surface of the catalyst. Toluene oxidation reaction path could be carried out in a continuous step. As shown in Fig. 8, the toluene molecule was adsorbed on the surface of catalysts, and reacted with the chemical adsorbed oxygen to form benzaldehydic species, eventually, formed $CO_2$ and $H_2O$. At the same time, the catalysts produced oxygen vacancies, and then $O_2$ molecular would replenish in the reaction gas to form the new chemical adsorbed oxygen. So, it completed the redox cycle.

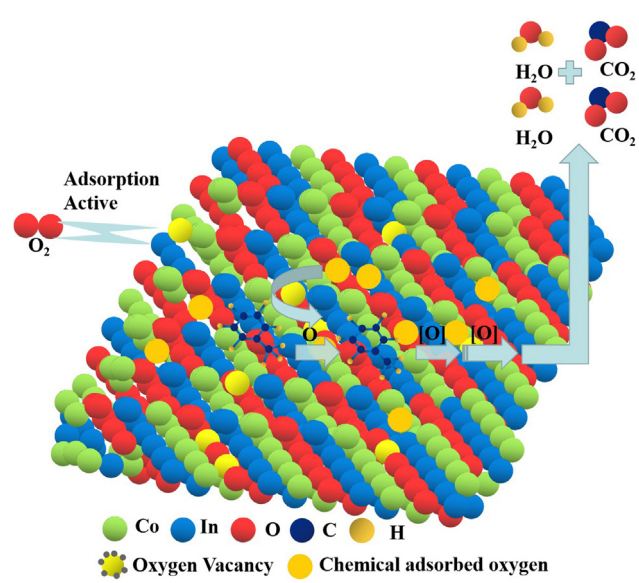


**Fig. 8** Schematic of toluene combustion on $Co_3O_4/In_2O_3$.

## 3. Conclusion

In summary, we synthesized a series of $Co_3O_4/In_2O_3$ catalysts with different Co/In molar ratio through the pyrolysis of ZIF-67/MIL-68, and the influence of Co/In molar ratio of $Co_3O_4/In_2O_3$ catalysts on the toluene oxidation was studied. From SEM image, the amount of *in situ* growth of $Co_3O_4$ nanododecahedra on $In_2O_3$ hexagonal prisms was diverse, obviously. Among the four $Co_3O_4/In_2O_3$ catalysts, the $Co_2In_1$ catalyst exhibited superior catalytic activity. The temperature for 90% toluene conversion ($T_{90}$) of $Co_2In_1$ catalyst was 182 °C. Meanwhile, the $Co_2In_1$ catalyst also exhibited good cycling at three consecutive runs and the excellent long-term thermal stability. Through various characterizations, it was concluded that the excellent catalytic performance of $Co_2In_1$ catalyst was attributed to the higher atomic ratio of $Co^{3+}/(Co^{3+}+Co^{2+})$ on the surface, lots of surface adsorbed oxygen, larger specific area and minimum crystallite size. In addition, this novel strategy could also open a door for the application of MOF materials to VOCs removal.

## Declaration of Competing Interest

The authors declare that they have no known competing financial interests or personal relationships that could have appeared to influence the work reported in this paper.

## Acknowledgements

This work was supported by the National Natural Science Foundation of China (21707145, 51908535), Key Science and Technology Program of Lanzhou City (2018-RC-65), Major Science and Technology Projects in Inner Mongolia Autonomous Region, Province Natural Science Foundation of GanSu (18JR3RA383), the Science and Technology Program of Chengguan district, Lanzhou city (2019JSCX0042).

## Appendix A. Supplementary data

Supplementary data to this article can be found online at https://doi.org/10.1016/j.arabjc.2020.01.014.

## References

Bahlawane, N., Tchoua Ngamou, P., Vannier, V., Kottke, T., Heberle, J., Kohse Höinghaus, K., 2009. Tailoring the properties and the reactivity of the spinel cobalt oxide. Phys. Chem. Chem. Phys. 11, 9224–9232.

Bai, B., Li, J., 2014. Positive Effects of $K^+$ Ions on Three-Dimensional Mesoporous Ag/ $Co_3O_4$ Catalyst for HCHO Oxidation. ACS Catal. 4, 2753–2762.

Bao, Y., Oh, W., Lim, T., Wang, R., Webster, R., Hu, X., 2018. Surface-nucleated heterogeneous growth of zeolitic imidazolate framework-A unique precursor towards catalytic ceramic membranes: Synthesis, characterization and organics degradation. Chem. Eng. J. 353, 69–79.

Cai, T., Deng, W., Dai, Q., Liu, W., Wang, X., 2015. Catalytic combustion of 1,2-dichlorobenzene at low temperature over Mn-modified $Co_3O_4$ catalysts. Appl. Catal. B: Environ. 166–167, 393–405.

Chen, X., Chen, X., Yu, E., Cai, S., Jia, H., Chen, J., Liang, P., 2018. In situ pyrolysis of Ce-MOF to prepare $CeO_2$ catalyst with obviously improved catalytic performance for toluene combustion. Chem. Eng. J. 344, 469–479.

Davies, T., Garcia, T., Solsona, B., Taylor, S., 2006. Nanocrystalline cobalt oxide: a catalyst for selective alkane oxidation under ambient conditions. Chem. Commun. 32, 3417–3419.

Delimaris, D., Ioannides, T., 2008. VOC oxidation over $MnO_x$-$CeO_2$ catalysts prepared by a combustion method. Appl. Catal. B: Environ. 84, 303–312.

Ding, S., Zhang, C., Liu, Y., Jiang, H., Xing, W., 2017. Pd nanoparticles supported on N-doped porous carbons derived from ZIF-67: Enhanced catalytic performance in phenol hydrogenation. J. Ind. Eng. Chem. 46, 258–265.

Du, Y., Meng, Q., Wang, J., Yan, J., Fan, H., Liu, Y., Dai, H., 2012. Three-dimensional mesoporous manganese oxides and cobalt oxides: High-efficiency catalysts for the removal of toluene and carbon monoxide. Microporous Mesoporous Mater. 162, 199–206.

Everaert, K., Baeyens, J., 2004. Catalytic combustion of volatile organic compounds. J. Hazard. Mater. 109, 113–139.

Feng, Y., Zheng, X., 2012. Copper Ion Enhanced Synthesis of nanostructured cobalt oxide catalyst for oxidation of methane. ChemCatChem 4, 1551–1554.

Garcia, T., Argouram, S., Sánchez-Royo, J., Murillo, R., Mastral, A., Aranda, A., Vázquez, I., Dejoz, A., Solsona, B., 2010. Deep oxidation of volatile organic compounds using ordered cobalt oxides prepared by a nanocasting route. Appl. Catal. A: Gen. 386, 16–27.

Han, W., Dong, F., Zhao, H., Tang, Z., 2018. Outstanding Water-resistance Pd-Co nanoparticles functionalized mesoporous carbon catalyst for CO catalytic oxidation at room temperature. Chemistryselect 3, 6601–6610.

Han, W., Zhao, H., Dong, F., Tang, Z., 2018. Morphology-controlled synthesis of 3D, mesoporous, rosette-like $CeCoO_x$ catalysts by pyrolysis of $Ce[Co(CN)_6]$ and application for the catalytic combustion of toluene. Nanoscale 10, 21307–21319.

He, C., Li, J., Cheng, J., Li, L., Li, P., Hao, Z., Xu, Z., 2009. Comparative Studies on Porous Material-Supported Pd Catalysts for Catalytic Oxidation of Benzene, Toluene, and Ethyl Acetate. Ind. Eng. Chem. Res. 48, 6930–6936.

Ji, Y., Zhao, Z., Duan, A., Jiang, G., Lin, J., 2009. Comparative Study on the Formation and Reduction of Bulk and $Al_2O_3$-Supported Cobalt Oxides by $H_2$-TPR Technique. J. Phys. Chem. C 113, 7186–7199.

Jin, L., Qian, X., Wanga, J., Aslan, H., Dong, M., 2015. MIL-68 (In) nano-rods for the removal of Congo red dye from aqueous solution. J. Colloid Interface Sci. 453, 270–275.

Jones, A., 1999. Indoor air quality and health. Atmos. Environ. 33, 4535–4564.

Kamal, M., Razzak, S., Hossain, M., 2016. Catalytic oxidation of volatile organic compounds (VOCs)-a review. Atmos. Environ. 140, 117–134.

Kampa, M., Castanas, E., 2008. Human health effects of air pollution. Environ. Pollut. 151, 362–367.

Kim, S., Shim, W., 2010. Catalytic combustion of VOCs over a series of manganese oxide catalysts. Appl. Catal. B: Environ. 98, 180–185.

Kołodziej, A., Łojewska, J., 2005. Optimization of structured catalyst carriers for VOC combustion. Catal. Today 105, 378–384.

Konsolakis, M., Carabineiro, S., Marnellos, G., Asad, M., Soares, O., Pereira, M., Órfão, J., Figueiredo, J., 2017. Effect of cobalt loading on the solid state properties and ethyl acetate oxidation performance of cobalt-cerium mixed oxides. J. Colloid. Interf. Sci. 496, 141–149.

Koo, W., Yu, S., Choi, S., Jang, J., Cheong, J., Kim, I., 2017. Nanoscale PdO catalyst functionalized $Co_3O_4$ hollow nanocages

using MOF templates for selective detection of acetone molecules in exhaled breath. ACS Appl. Mater. Inter. 9, 8201–8210.

Li, L., Liu, S., Liu, J., 2011. Surface modification of coconut shell based activated carbon for the improvement of hydrophobic VOC removal. J. Hazard. Mater. 192, 683–690.

Li, W., Wang, J., Gong, H., 2009. Catalytic combustion of VOCs on non-noble metal catalysts. Catal. Today 148, 81–87.

Li, G., Zhang, C., Wang, Z., Huang, H., Peng, H., Li, X., 2018. Fabrication of mesoporous $Co_3O_4$ oxides by acid treatment and their catalytic performances for toluene oxidation. Appl. Catal. A: Gen. 550, 67–76.

Liu, Y., Dai, H., Deng, J., Xie, S., Yang, H., Tan, W., Jiang, Y., Guo, G., 2014. Mesoporous $Co_3O_4$-supported gold nanocatalysts: Highly active for the oxidation of carbon monoxide, benzene, toluene, and o-xylene. J. Catal. 309, 408–418.

Lou, Y., Wang, L., Zhang, Y., Zhao, Z., Zhang, Z., Lu, G., Guo, Y., 2011. The effects of $Bi_2O_3$ on the CO oxidation over $Co_3O_4$. Catal. Today 175, 610–614.

Lou, Y., Ma, J., Cao, X., Wang, L., Dai, Q., Zhao, Z., Cai, Y., Zhan, W., Guo, Y., Hu, P., Lu, G., Guo, Y., 2014. Promoting Effects of $In_2O_3$ on $Co_3O_4$ for CO Oxidation: Tuning $O_2$ Activation and CO Adsorption Strength Simultaneously. ACS Catal. 4, 4143–4152.

Lou, Y., Cao, X., Lan, J., Wang, L., Dai, Q., Guo, Y., Ma, J., Zhao, Z., Guo, Y., Hu, P., Lu, G., 2014. Ultralow-temperature CO oxidation on an $In_2O_3$-$Co_3O_4$ catalyst: a strategy to tune CO adsorption strength and oxygen activation simultaneously. Chem. Commun. 50, 6835–6838.

Luo, Y., Zheng, Y., Zuo, J., Feng, X., Wang, X., Zhang, T., Zhang, K., Jiang, L., 2018. Insights into the high performance of Mn-Co oxides derived from metal-organic frameworks for total toluene oxidation. J. Hazard. Mater. 349, 119–127.

Ma, L., Seo, C., Chen, X., Sun, K., Schwank, J., 2018. Indium-doped $Co_3O_4$ nanorods for catalytic oxidation of CO and $C_3H_6$ towards diesel exhaust. Appl. Catal. B: Environ. 222, 44–58.

Malhautier, L., Quijano, G., Avezac, M., Rocher, J., Fanlo, J., 2014. Kinetic characterization of toluene biodegradation by Rhodococcus erythropolis: towards a rationale for microflora enhancement in bioreactors devoted to air treatment. Chem. Eng. J. 247, 199–204.

Marcos, F., Casilda, V., BaÇares, M., Fernandez, J., 2013. Control of the Interphases Formation Degree in $Co_3O_4$/ZnO Catalysts. ChemCatChem 5, 1431–1440.

Papaefthimiou, P., Ioannides, T., Verykios, X., 1997. Combustion of non-halogenated volatile organic compounds over group VIII metal catalysts. Appl. Catal. B: Environ. 13, 175–184.

Ren, Q., Mo, S., Peng, R., Feng, Z., Zhang, M., Chen, L., Fu, M., Wu, J., Ye, D., 2018. Controllable synthesis of 3D hierarchical $Co_3O_4$ nanocatalysts with various morphologies for the catalytic oxidation of toluene. J. Mater. Chem. A. 6, 498–509.

Ruddy, E.N., Carroll, L.A., 1993. Select the Best VOC Control strategy. Chem. Eng. Prog. 88, 28–35.

Santos, S., Jones, K., Abdul, R., Boswell, J., Paca, J., 2007. Treatment of Wet Process Hardboard Plant VOC Emissions by a Pilot Scale Biological System. Biochem. Eng. J. 37, 261–270.

Shang, Z., Sun, M., Chang, S., Che, X., Cao, X., Wang, L., Guo, Y., Zhan, W., Guo, Y., Lu, G., 2017. Activity and stability of $Co_3O_4$-based catalysts for soot oxidation: The enhanced effect of $Bi_2O_3$ on activation and transfer of oxygen. Appl. Catal. B: Environ. 209, 33–44.

Shi, Q., Chen, Z., Song, Z., Li, J., Dong, J., 2011. Synthesis of ZIF-8 and ZIF-67 by steam-assisted conversion and an investigation of their tribological behaviors. Angew. Chem. Int. Ed. 50, 672–675.

Tang, W., Wu, X., Li, S., Li, W., Chen, Y., 2014. Porous Mn-Co mixed oxide nanorod as a novel catalyst with enhanced catalytic activity for removal of VOCs. Catal. Commun. 56, 134–138.

Tokumura, M., Nakajima, R., Znad, H.T., Kawase, Y., 2008. Chemical Absorption Process for Degradation of VOC Gas Using Heterogeneous Gas-Liquid Photocatalytic Oxidation: Toluene Degradation by Photo-Fenton Reaction. Chemosphere 73, 768–775.

Tsai, C., Langner, E., 2016. The effect of synthesis temperature on the particle size of nano-ZIF-8. Micropor. Mesopor. Mater. 221, 8–13.

Wang, X., Zhong, W., Li, Y., 2015. Nanoscale Co-based catalysts for low-temperature CO oxidation. Catal. Sci. Technol. 5, 1014–1020.

Wang, X., Liu, Y., Zhang, T., Luo, Y., Lan, Z., Zhang, K., Zuo, J., Jiang, L., Wang, R., 2017. Geometrical-site-dependent catalytic activity of ordered mesoporous Co-based spinel for benzene oxidation: In situ DRIFTS Study coupled with Raman and XAFS spectroscopy. ACS Catal. 7, 1626–1636.

Wei, T., Chen, C., Chien, H., Lu, S., Hu, C., 2010. A cost-effective supercapacitor material of ultrahigh specific capacitances: spinel nickel cobaltite aerogels from an epoxide-driven sol-gel process. Adv. Mater. 22, 347–351.

Wu, R., Qu, J., He, H., Yu, Y., 2004. Removal of azo-dye Acid Red B (ARB) by adsorption and catalytic combustion using magnetic $CuFe_2O_4$ powder. Appl. Catal. B: Environ. 48, 49–56.

Xie, X., Shen, W., 2009. Morphology control of cobalt oxide nanocrystals for promoting their catalytic performance. Nanoscale. 1, 50–60.

Yan, L., Ren, T., Wang, X., Ji, D., Suo, J., 2003. Catalytic decomposition of $N_2O$ over $M_xCo_{1-x}Co_2O_4$ (M = Ni, Mg) spinel oxides. Appl. Catal. B: Environ. 45, 85–90.

Yang, H., Dai, H., Deng, J., Xie, S., Han, W., Tan, W., Jiang, Y., Au, C., 2014. Porous Cube-Aggregated $Co_3O_4$ Microsphere-Supported Gold Nanoparticles for Oxidation of Carbon Monoxide and Toluene. ChemSusChem 7, 1745–1754.

Yang, Q., Vaesen, S., Vishnuvarthan, M., Ragon, F., Serre, C., Vimont, A., Daturi, M., Weireld, G., Maurin, G., 2012. Probing the adsorption performance of the hybrid porous MIL-68 (Al): a synergic combination of experimental and modelling tools. J. Mater. Chem. 22, 10210–10220.

Zhao, J., Han, W., Dong, F., Zhang, J., Tang, Z., 2018. Solvothermal systhesis of size-controlled porous $Co_3O_4$ nanostructure catalyst and their catalytic properties for VOCs removal. Chemistryselect 3, 10408–10417.

Zhao, J., Dong, F., Han, W., Zhang, J., Tang, Z., 2019. Controlled porous hollow $Co_3O_4$ polyhedral nanocages derived from metal-organic frameworks (MOFs) for toluene catalytic oxidation. Mol. Catal. 463, 77–86.

Zhao, J., Dong, F., Han, W., Zhang, J., Tang, Z., 2019. Carefully design hollow $Mn_xCo_{3-x}O_4$ polyhedron derived by Mn@Co-ZIFs and applied to catalytic oxidation of VOCs. Cryst. Growth Des. 19, 6207–6217.

Zhao, Z., Lin, X., Jin, R., Wang, G., Muhammad, T., 2012. $MO_x$ (M = Mn, Fe, Ni or Cr) improved supported $Co_3O_4$ catalysts on ceria–zirconia nanoparticulate for CO preferential oxidation in $H_2$-rich gases. Appl. Catal. B: Environ. 115–116, 53–62.